

# Controlled Synthesis of ZnO Nanostructures for Sub-ppm Level VOC Detection

Shao-Lin Zhang, Hyung-Gi Byun, Jeong-Ok Lim, Jeung-Soo Huh, and Wooyoung Lee

**Abstract**—Various ZnO nanostructures including nanoparticles, nanorods, nanotubes, and nanorings were controlled synthesized by a facile sonochemical method combined with a chemical etching process. The morphology and structure of the fabricated nanomaterials were characterized by X-ray diffraction (XRD), scanning electron microscopy (SEM), and transmission electron microscopy (TEM). The sensing properties of different ZnO nanostructures towards volatile organic compounds VOC gases at sub-ppm levels were investigated. The differences in sensing responses of various nanostructures were compared and reasonable mechanisms are proposed here.

**Index Terms**—ZnO nanomaterials, Controlled synthesis, VOC gas sensor

## I. INTRODUCTION

NANOSTRUCTURED ZnO is a promising material for chemical gas sensors because of its large surface-to-volume ratio and high porosity, which improve its sensitivity and response speed [1-3]. Recently, ZnO gas sensors have been studied extensively due to their simplicity of preparation and high chemical stability. Furthermore, ZnO gas sensors have been prepared by different methods, such as oxidation of Zn metal [4], radio frequency (RF) sputtering [5-8], sol-gel [9-15], hydrothermal processing [16-20], chemical vapor deposition [21-24], electrochemical methods [25, 26], and ultrasonic atomization techniques [27].

Many studies had focused on the synthesis and volatile

organic compound (VOC) gas sensing properties of various ZnO nanostructures. Bai et al. fabricated nanostructured films of tetrapod-shaped ZnO by a combination of screen-printing technology and hydrothermal treatment. The tetrapod-shaped ZnO exhibited excellent responses ( $R_a/R_g$ ) as high as 6.5 and 14 to 100 ppm benzene and toluene at 430°C, respectively [28]. ZnO nanopillar sensor had been prepared by Bie et al. using a two-step solution method. The response ( $R_a/R_g$ ) of the ZnO nanopillar sensor reached 18.29 for 100 ppm ethanol at 350°C [29]. However, considering the strict indoor leakage standard of VOC gases, the detection limits in these studies are still high. Furthermore, the operating temperatures of these ZnO nanomaterials sensors are relatively high, which restricts the practical application and reduces the long-term stability of the sensors. As such, it is desirable to systematically investigate ZnO nanostructures to obtain high sensitivity as well as rapid response and recovery in the presence of low concentrations of VOC gases at relatively low operating temperatures.

Previous investigations have shown that the sensing performance of ZnO nanomaterials is highly dependent on their micro-morphologies [30-34]. It is necessary to explore the sensing properties of ZnO with different nanostructures to determine the optimal nanostructures for VOC gas detection through a systematic study of the morphology-property relationship. For this purpose, we developed technologies for the controlled synthesis of various kinds of ZnO nanostructures via a sonochemical method combined with chemical etching. The obtained ZnO nanoparticles (ZNPs), nanorods (ZNRDs), nanotubes (ZNTs), and nanorings (ZNRs) were used to fabricate MEMS sensors, which were tested using four kinds of VOC gases (toluene, benzene, acetaldehyde, and formaldehyde). The temperature-dependent and concentration-dependent sensing characterizations of the different ZnO nanostructures were studied and compared. The results revealed that the ZNRs exhibited the best sensitivity toward VOC gases among the various ZnO nanostructures. Moreover, the detection limit of the ZNR sensors toward VOC gases was down to the sub-ppm level.

## II. EXPERIMENTAL

### A. Preparation and characterization of sensor materials

ZNRDs and ZNPs were synthesized by the sonochemical method using zinc nitrate hydrate ( $Zn(NO_3)_2 \cdot 6H_2O$ ) and hexamethylenetetramine (HMT,  $C_6H_{12}N_4$ , also known as methenamine) as starting materials at room temperature without any surfactant, catalyst or template. In a typical

Manuscript received August 1, 2011. This research was supported by the Priority Research Centers Program through the National Research Foundation of Korea (NRF) funded by the Ministry of Education, Science and Technology (2009-0093823), Republic of Korea.

Shao-Lin Zhang is with the Department of Materials Science and Engineering, Yonsei University, Seoul, 120749 Republic of Korea (e-mail: slzhang@yonsei.ac.kr).

Hyung-Gi Byun is with the Department of Information and Communication, Kangwon National University, Samcheok, 245711 Republic of Korea (e-mail: byun@kangwon.ac.kr).

Jeong-Ok Lim is with Biomedical Research Institute, Kyungpook National University, Daegu, 702701 Republic of Korea (email: jolim@knu.ac.kr)

Jeung-Soo Huh is with the School of Materials Science and Metallurgy, Kyungpook National University, Daegu, 702701 Republic of Korea (e-mail: jshuh@knu.ac.kr).

Wooyoung Lee is with the Department of Materials Science and Engineering, Yonsei University, Seoul, 120749 Republic of Korea (phone: 82-2-2123-2834; fax: 82-2-312-5375; e-mail: wooyoung@yonsei.ac.kr).

Copyright (c) 2012 IEEE. Personal use of this material is permitted. However, permission to use this material for any other purposes must be obtained from the IEEE by sending a request to pubs-permissions@ieee.org.

process, a 100 ml aqueous solution of  $\text{Zn}(\text{NO}_3)_2 \cdot 6\text{H}_2\text{O}$  and a 100 ml aqueous solution of HMT at equivalent concentrations were mixed together and kept under vigorous magnetic stirring for 10 min. Two precursor concentrations (0.1 M and 0.01 M) were used to control the morphology of the products. Subsequently, the solutions were irradiated by intense ultrasound with an irradiation power of 500 W for 90 min under ambient conditions. The ultrasonic treatment was performed using an ultrasonic processor (VCX 750, Sonics & Materials) with a 0.5-inch horn made of a titanium alloy producing an ultrasonic frequency of 20 kHz. After irradiation, the transparent solutions changed to white suspensions. The white precipitates were then centrifuged, washed with distilled water and ethanol several times to remove ionic impurities, and were finally dried in a vacuum at room temperature. Finally, ZNPs and ZNRDs were obtained after ultrasonic irradiation of the 0.1 M and 0.01 M solutions, respectively.

ZNTs (or ZNRs) were fabricated by chemical etching of ZNRDs (or ZNPs). The ZNRD (or ZNP) powder was mixed with a proper volume of ethanol and vigorously stirred for 10 min. The resulting suspension was then added dropwise to 50 ml of NaOH solution (1.5 M) at room temperature. After constant magnetic stirring for six hours, the white powder was centrifuged, washed and dried in a vacuum, and finally ZNTs (or ZNRs) were obtained.

The as-prepared samples were characterized by X-ray diffraction (XRD, Cu K) to observe the structural nature. The XRD patterns were recorded from  $10^\circ$  to  $80^\circ$  ( $2\theta$ ) with a scanning step of  $0.02^\circ$ . The morphologies of the samples were analyzed by field-emission scanning electron microscopy (FE-SEM, Hitachi S-4300) operated at 15 KeV. The transmission electron microscope (TEM) and selected area electron diffraction (SAED) images were obtained using a Hitachi H7600 transmission electron microscope at an acceleration voltage of 100 kV.

### B. Fabrication of MEMS sensor

In order to minimize the power consumption, micro sensor substrates were developed using MEMS technology. The MEMS substrates were fabricated on 4-in., 300- $\mu\text{m}$ -thick Si wafers. A structural stack ( $\text{Si}_3\text{N}_4$ ) was first deposited on the wafers by low pressure chemical vapor deposition (LPCVD). Then, platinum was deposited using a sputtering method with a patterned mask. After removing the mask, a patterned micro-heater and electrode were obtained. The micro-heater and electrode were formed in a single metallization reaction, leading to an increase in device reliability. This technique prevents the overlap of metal tracks, which would require dielectric insulating layers able to withstand repeated thermal cycles at high temperature. A silicon dioxide passivation layer was deposited on top of the metallized platinum to electrically insulate the sensing electrode from the micro-heater. Finally, the backside of the substrate was removed using a micromachining method. The fabricated MEMS substrate is shown in Fig. 1 (a). The dimensions of the substrate are 1.8 mm x 1.8 mm with a 400  $\mu\text{m}$  x 400  $\mu\text{m}$  sensing area. The gap distance between the two electrodes is 70  $\mu\text{m}$ , and the

resistance of the micro-heater is about 30  $\Omega$ .

The obtained sensor materials were mixed with ethylcellulose and  $\alpha$ -terpineol (wt. 1:20) to form mud pastes. The pastes were then coated onto the MEMS substrates using a dropping method. Subsequently, the fabricated MEMS sensors were dried at  $90^\circ\text{C}$  for 2 h and annealed at  $600^\circ\text{C}$  for 1 h. The drying process was used to prevent an explosion during subsequent high temperature heating, while the annealing treatment was used to remove the impurities and improve the stability of the sensors.

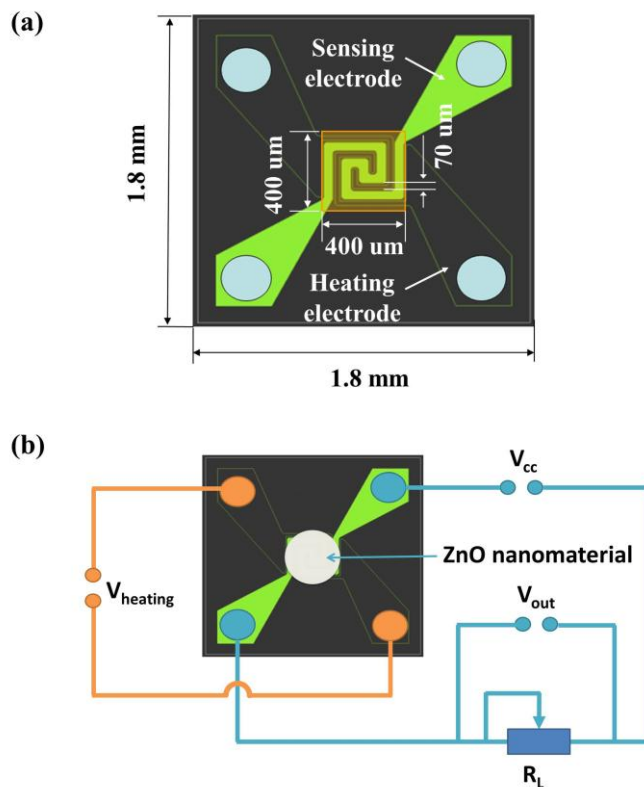


Fig. 1. (a) Structure and dimensions of the MEMS sensor platform, and (b) equivalent circuit for gas sensor measurement.

### C. VOC sensing test

The prepared MEMS sensor was soldered with a tetrapod holder by a wire bonding process and covered by a meshed cap. Then, the sensor was put into a test chamber with a total volume of 5  $\text{cm}^3$ . Synthetic dry air at a constant flow rate of 250 sccm acted as a carrier gas. Manufactured standard VOC gases were diluted in nitrogen (Daehan Gas Co., Ltd.) including toluene (50 ppm), benzene (50 ppm), acetaldehyde (5 ppm) and formaldehyde (5 ppm), and were used as target gases. The desired concentrations of the VOC gases were obtained from certified cylinders and a mixing system with mass flow controllers and mass flow meters. The equivalent circuit for gas sensor measurement is shown in Fig. 1(b), where  $V_{\text{heating}}$  represents the voltage supplied to the heater, and  $V_{\text{cc}}$  represents the applied voltage ( $V_{\text{cc}} = 4$  V). The sensor signal ( $V_{\text{out}}$ ) was obtained from the voltage variation across the reference resistance under air or VOC gas exposure. The actual resistance of the sensor ( $R_S$ ) can be calculated from the output voltage

( $V_{out}$ ) by the following equation:

$$R_S = R_L \frac{V_{cc} - V_{out}}{V_{out}} \quad (1)$$

Then the sensing response is defined as

$$S = \frac{R_a}{R_g} \quad (2)$$

where  $R_a$  and  $R_g$  represent the resistance of the MEMS sensor upon exposure to air and the target gas, respectively.

### III. RESULTS AND DISCUSSION

#### A. Characterization of sensor materials

XRD measurements were performed to determine the crystal structure and phase purity of the products. Fig. 2 shows the XRD patterns of the ZNPs, ZNRDs, ZNTs and ZNRs. All of the diffraction peaks can be indexed as wurtzite hexagonal ZnO with lattice constants of  $a = 0.325$  nm and  $c = 0.521$  nm, which are consistent with the values in the standard card (JCPDS 36-1451). The strong diffraction peaks indicate that the ZnO is of a highly crystallized form. No characteristic peaks are observed for other impurities, indicating the products have high purity.

The general morphologies of the as-synthesized ZNPs and ZNRDs are shown in Fig. 3. Fig. 3 (a) and (b) present low resolution SEM images of ZNPs and ZNRDs, respectively, showing that large-scale nanoparticles and nanorods are produced in our experiment. The obtained nanomaterials are well dispersed with uniform size. The average diameter of the ZNRDs is around 180 nm, while the length is in the range of 1000-1500 nm. The inset images show that the ZNPs and ZNRDs have a well-defined hexagonal cross-section. Fig. 3 (c) is a TEM image of a nanorod, which is well consistent with the SEM observations. Fig. 3 (d) shows a high resolution TEM (HRTEM) image of the corresponding nanorods, revealing that the nanorods grew along the [0001] direction. The inset of Fig. 3 (d) presents the corresponding SAED pattern, which further verifies the single crystalline nature of the product.

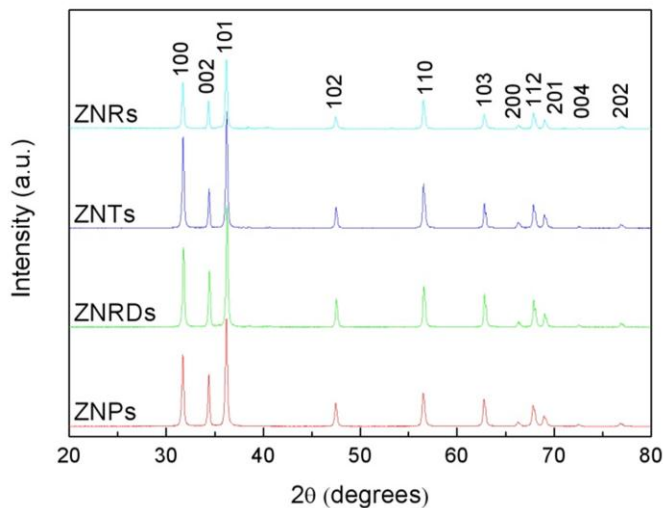


Fig. 2. XRD patterns of ZnO nanoparticles, nanorods, nanotubes and nanorings.

SEM images of the ZNTs and ZNRs are shown in Fig. 4 (a) and (c), respectively. It is apparent that hollow structures are

formed in the inner part of ZNRDs and ZNPs after the chemical etching process. As shown in the insets, the ZNTs and ZNRs have a hexagonal cross-section with inner diameters of 60 nm and 120 nm, respectively, while the external diameter and length are similar to those of the nanorods and nanoparticles, respectively. The TEM image of ZNTs in Fig. 4 (b) reveals that the ZNTs are not completely tubular, i.e., part of the ZNT is hollow, and the rest remains a rod. Fig. 4 (d) shows a TEM image of ZNRs, in which a perfect ring-like structure is observed.

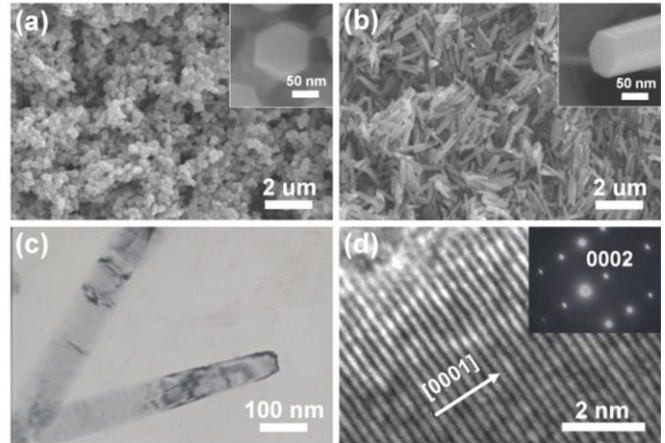


Fig. 3. SEM images of ZnO (a) nanoparticles and (b) nanorods; the insets are the corresponding hexagonal tip. (c) TEM image and (d) high-resolution TEM image of ZnO nanorods; the inset in (d) is the corresponding SAED pattern.

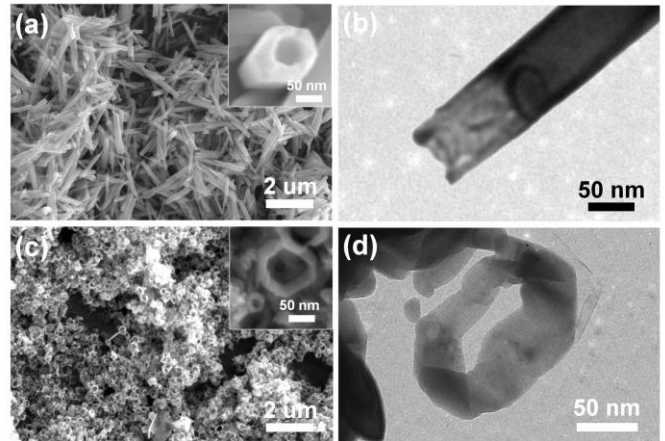


Fig. 4. (a) SEM image of ZnO nanotubes; the inset is a hexagonal tube tip. (b) TEM image of ZnO nanotubes showing the hollow structure inside the nanotubes. (c) SEM image of ZnO nanorings; the inset shows the hexagonal ring-like structure. (d) TEM image of ZnO nanorings.

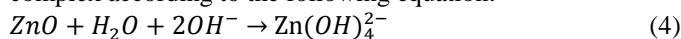
The formation mechanisms of different ZnO nanostructures are simply depicted as follows. First, the HMT in the precursor solution decomposes into  $\text{OH}^-$  under ultrasonic irradiation. The  $\text{OH}^-$  then combines with  $\text{Zn}^{2+}$  to form soluble  $\text{Zn}(\text{OH})_4^{2-}$ . With intense ultrasonic irradiation,  $\text{Zn}(\text{OH})_4^{2-}$  is split and form ZnO according to Eq. (3):



where the symbol ))) represents the ultrasonic irradiation. Different from the results generated with the hydrothermal method, where the higher precursor concentration generally

leads to longer or larger morphology [35], our experiment shows a contrary result. This is because the extremely high temperature and pressure created by ultrasonic irradiation greatly enhance the nucleus formation in the initial stage of growth. When the high-intensity ultrasound was irradiated in the precursor with high concentration, the massive nucleation exhausted the  $Zn^{2+}$  in the solution. The lack of  $Zn^{2+}$  source stunted the further growth of ZNPs. This effect weakens as the precursor concentration decreases, leading to the growth of ZNRDs in the lower concentration solution.

When the ZNPs and ZNRDs were immersed into the alkaline solution, the inverse reaction of Eq. (3) took place. The ZnO was dissolved by the  $OH^-$  anions and formed a soluble hydroxyl complex according to the following equation:



The dissolution first occurred in the central part, and then extended to the inner and outer part of the ZNPs and ZNRDs. This preferential etching is attributed to the inhomogeneous existence of defects in the ZNPs and ZNRDs [36, 37].

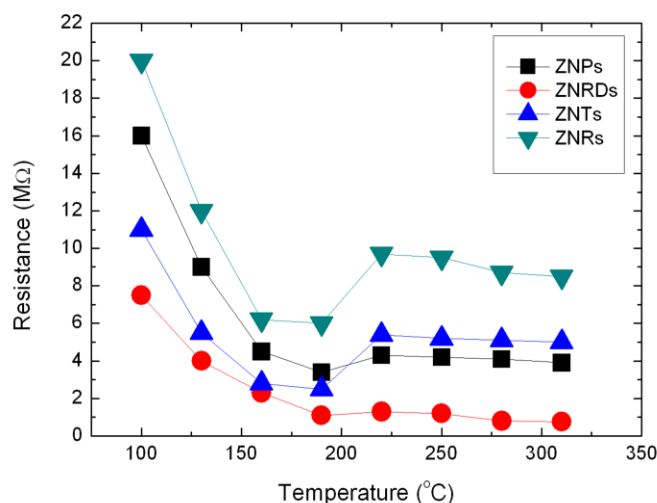


Fig. 5. Temperature dependent resistances of ZnO nanomaterials-based MEMS sensors.

### B. Sensing properties

The temperature-dependent electroconductivity of various ZnO nanostructures was also investigated. Fig. 5 depicts the resistances of ZnO nanomaterial sensors depending on the operating temperature, ranging from 100°C to 310°C. The resistance of the sensing materials first decreased as the operating temperature increased, owing to the semiconducting behavior of the metal oxide. With a further increase in temperature, an increase in resistance was observed at an operating temperature ranging from 190°C to 220°C. This increase in resistance is attributed to the extraction of free electrons caused by the vigorous oxygen adsorption on the ZnO nanomaterials. In a temperature range higher than 220°C, the resistance decreased again, probably because of the dominant thermal excitation of electrons and desorption of oxygen species [38]. Similar phenomena have been observed in other studies [39]. However, it is noteworthy that the increases in the resistance of ZNTs and ZNRs were much larger than those of

ZNPs and ZNRDs in the temperature range from 190°C to 220°C. It can be inferred that the impact of oxygen absorption is greatly enhanced due to the large specific surface area induced by the special hollow structures in ZNTs and ZNRs.

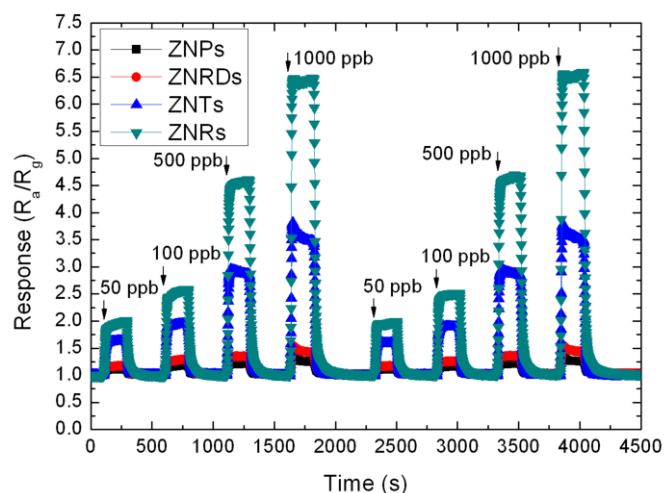


Fig. 6. Dynamic response of ZnO nanomaterial-based MEMS sensors towards different concentrations of acetaldehyde at 220°C.

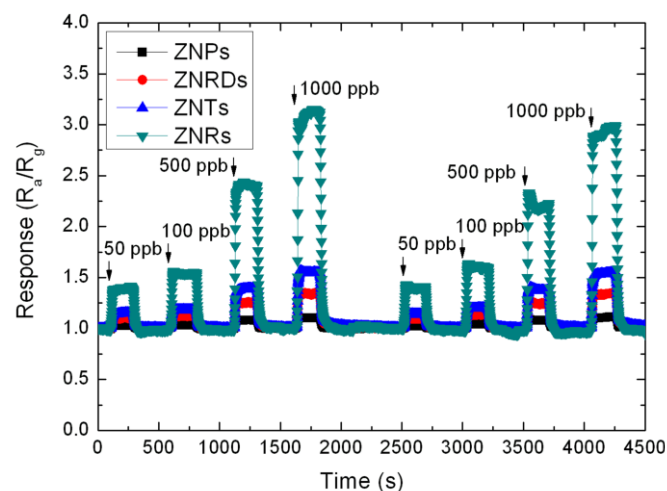


Fig. 7. Dynamic response of ZnO nanomaterial-based MEMS sensors towards different concentrations of formaldehyde at 220°C.

Fig. 6 shows the dynamic response of ZnO nanomaterial-based MEMS sensors toward acetaldehyde at concentrations ranging from 50 ppb to 1 ppm. The sensors responded quickly upon exposure to acetaldehyde at 220°C. After removing the acetaldehyde, the response of the sensors recovered 100%. The response of the sensors increased with increasing target gas concentration. Furthermore, ZNRs sensors performed the greatest response among the four kinds of nanostructures. The ZNT sensor had almost half the response comparing to the ZNR sensor, and the ZNRD and ZNP sensors showed a relatively low response. ZnO nanomaterial sensors also were investigated using a similar test with formaldehyde. Fig. 7 shows the dynamic response of the ZnO nanomaterial sensors in the presence of different concentrations of

formaldehyde. The sensors showed good responses toward formaldehyde. Similar to the test for acetaldehyde, the ZNR sensor exhibited higher sensitivity than the other three nanostructures.

Fig. 8 and Fig. 9 show the response of ZnO nanomaterial sensors toward benzene and toluene. The responses of sensors corresponded well to the increase in gas concentration. Moreover, the response increased linearly to the benzene and toluene as the concentration increased from 500 ppb to 20 ppm.

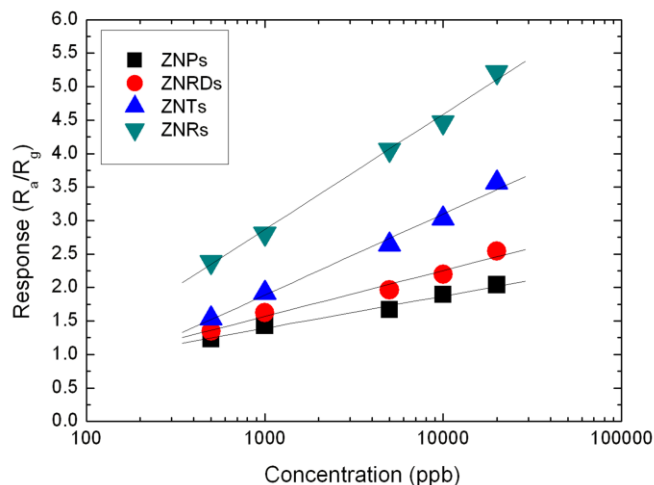


Fig. 8. Response of ZnO nanomaterial-based MEMS sensors towards various concentrations of benzene at 220°C.

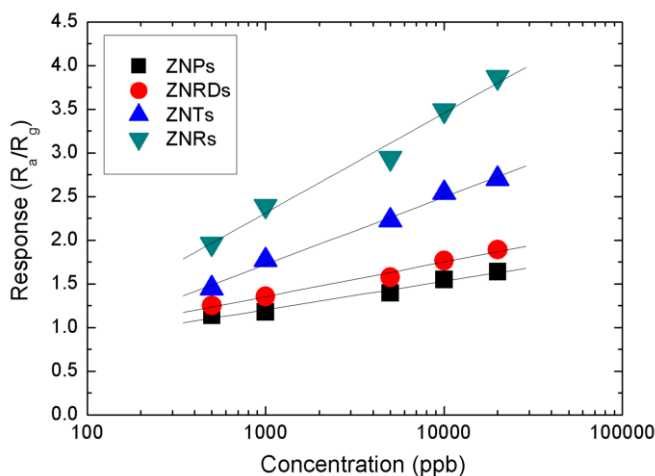
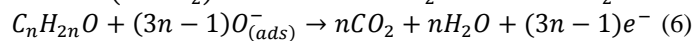


Fig. 9. Response of ZnO nanomaterial-based MEMS sensors towards various concentrations of toluene at 220°C.

It is well known that oxygen molecules adsorb on the surface of the nanostructured ZnO at elevated temperature to form  $O_2^-$ ,  $O^-$ ,  $O^{2-}$  ions by capturing electrons from the conduction band, and thus reduce the electric conductivity. When the sensor materials are exposed to the VOC gases, the reducing gases react with the adsorbed oxygen and, as a result, captured electrons are released to the conduction band. This process eventually increases the electric conductivity of ZnO sensors [40, 41]. The overall reaction of VOC gases with adsorbed oxygen species can be explained based on the following reactions:



where  $C_mH_n$  denotes benzene and toluene, and  $C_nH_{2n}O$  represents formaldehyde and acetaldehyde. After the reaction, the VOC gases are decomposed and oxidized to  $CO_2$  and  $H_2O$ .

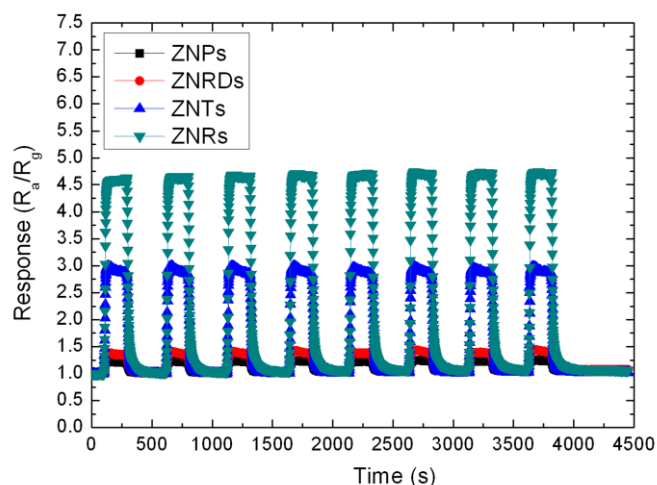


Fig. 10. Reproducibility of ZnO nanomaterial-based MEMS sensors towards 500 ppb of acetaldehyde at 220°C.

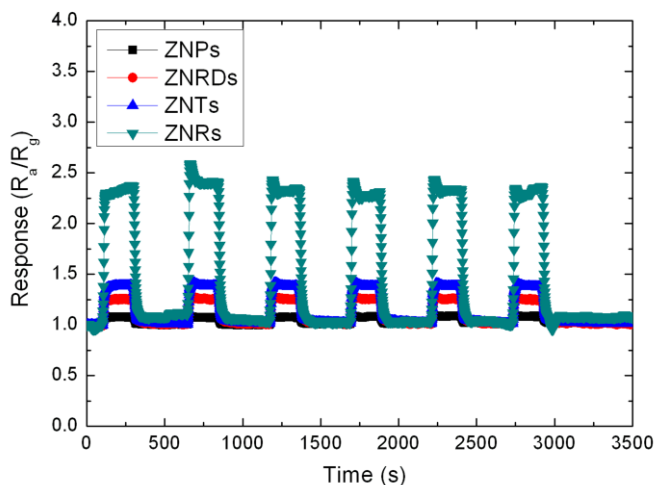


Fig. 11. Reproducibility of ZnO nanomaterial-based MEMS sensors towards 500 ppb of formaldehyde at 220°C.

It was found the sensor responses to VOC gases were in the following order for all tests: ZNR > ZNT > ZNRD > ZNP. The large surface area of the hollow structured ZNRs and ZNTs greatly increased the number of adsorptive sites for oxygen molecules. Further, the existence of abundant defects caused by the etching process also greatly increased the reactive sites in the sensor materials. Consequently, the ZNR and ZNT sensors exhibited much higher sensitivity compared to the ZNRDs and ZNPs. Furthermore, the wholly hollow ring-like structure not only has increased surface area, but also enhanced the diffusion of VOC gas molecules in the sensing layer. The enhanced gas diffusion facilitated the completed reaction of VOC gas molecules, and thus further increased the effective surface area of the sensor material. As a result, the ZNR sensor showed the best performance in our tests. It is also believed that the

relatively smaller sensitivity of ZNPs is due to the densely packed structure of the sensing layer, which obstructs the diffusion of VOC gas molecules. In comparison, ZNRDs with a high aspect ratio tend to pack loosely, facilitating gas diffusion in the sensing layer. As a result, ZNRD sensors exhibited a better sensitivity than ZNPs.

The reproducibility of ZnO nanomaterial-based MEMS sensor detection was also investigated. Fig. 10 and Fig. 11 show the repeated response of the MEMS sensors towards 500 ppb acetaldehyde and formaldehyde, respectively. The tests were repeated over six times. No variance in response was observed, revealing that our MEMS sensors have excellent reproducibility.

#### IV. CONCLUSION

In summary, ZnO nanoparticles, nanorods, nanotubes, and nanorings were successfully synthesized using facile sonochemical treatment combined with chemical etching. The obtained ZnO nanostructures were coated on micro sensor substrates fabricated by MEMS technology. The sensing properties of these MEMS sensors toward benzene, toluene, formaldehyde, and acetaldehyde were investigated and compared. The sensors exhibited excellent sensitivity toward the VOC gases at sub-ppb levels. High repeatability and switching behavior of the sensors were also observed. The ZnO nanoring sensor showed the highest sensitivity among the four kinds of ZnO nanostructures. The excellent response of the ZnO nanorings is due to its special ring-like structure, which increases the surface area and enhances gas diffusion.

#### REFERENCES

- [1] C.Y. Lu, S. P. Chang, S. J. Chang, T. J. Hsueh, C. L. Hsu, Y. Z. Chiou, I. C. Chen, *IEEE Sens. J.* 9 (4), 485, 2009.
- [2] B. L. Zhu, D. W. Zeng, J. Wu, W. L. Song, C. S. Xie, *J. Mater. Sci. Mater. Electron* 14, 521, 2003.
- [3] D. Mishra, A. Srivastava, A. Srivastava, R. K. Shukla, *Appl. Surf. Sci.* 55, 2947, 2008.
- [4] T. J. Hsueh, C. L. Hsu, *Sens. Actuators B* 131, 572, 2008.
- [5] C. Supab, H. Niyom, M. Pongsri, M. Nikorn, *Physica E* 39, 53, 2007.
- [6] X. Zhou, Q. Xue, M. Ma, J. Li, *Thin Solid Films* 519, 6151, 2011.
- [7] Y.S. Yoon, *Ceram. Int.*, doi:10.1016/j.ceramint.2011.05.128, 2011.
- [8] X. Zhou, Q. Xue, H. Chen, C. Liu, *Physica E* 42, 2021, 2010.
- [9] D. F. Paraguay, M. Miki-Yoshida, J. Morales, J. Solis, L. W. Estrada, *Thin Solid Films* 373, 137, 2000.
- [10] H. W. Ryu, B. S. Park, S. A. Akbar, W. S. Lee, K. J. Hong, Y. J. Seo, D. C. Shin, J. S. Park, G. P. Choi, *Sens. Actuators B* 96, 717, 2003.
- [11] N. Kakati, S. H. Jee, S. H. Kim, J. Y. Oh, Y. S. Yoon, *Thin Solid Films* 519, 494, 2010.
- [12] G. Sarala Devi, V. Bala Subrahmanyam, S. C. Gadkari, S. K. Gupta, *Analytica Chimica Acta* 568, 41, 2006.
- [13] P. Bhattacharyya, P. K. Basu, H. Saha, S. Basu, *Sens. Actuators B* 124, 62, 2007.
- [14] X. L. Cheng, H. Zhao, L. H. Huo, S. Gao, J. G. Zhao, *Sens. Actuators B* 102, 248, 2004.
- [15] C. Ge, Z. Bai, M. Hu, D. Zeng, S. Cai, C. Xie, *Mater. Lett.* 62, 2307, 2008.
- [16] C. J. Chang, S. T. Hung, C. K. Lin, C. Y. Chen, E. H. Kuo, *Thin Solid Films* 519, 1693, 2010.
- [17] J. Q. Xu, Y. P. Chen, D. Y. Chen, J. N. Shen, *Sens. Actuators B* 113, 526, 2006.
- [18] B. Baruwati, D. K. Kumar, S. V. Manorama, *Sens. Actuators B* 119, 676, 2006.
- [19] Y. Zeng, T. Zhang, L. Qiao, *Mater. Lett.* 63, 843, 2009.
- [20] Y. Zeng, T. Zhang, M. Yuan, M. Kang, G. Lu, R. Wang, H. Fan, Y. He, H. Yang, *Sens. Actuators B* 143, 93, 2009.

- [21] D. Barreca, D. Bekermann, E. Comini, A. Devi, R. A. Fischer, A.o Gasparotto, C. Maccato, G. Sberveglieri, E. Tondello, *Sens. Actuators B* 149, 1, 2010.
- [22] S. O'Brien, M. G. Nolan, M. Çopuroglu, J. A. Hamilton, I. Povey, L. Pereira, R. Martins, E. Fortunato, M. Pemble, *Thin Solid Films* 518, 4515, 2010.
- [23] F. S. Chien, C. R. Wang, Y. L. Chan, H. L. Lin, M. H. Chen, R. J. Wu, *Sens. Actuators B* 144, 120, 2010.
- [24] A. Dutta, T. K. Chaudhuri, S. Basu, *Mater. Sci. Eng., B* 14, 31, 1992.
- [25] P. K. Basu, P. Bhattacharyya, N. Saha, H. Saha, S. Basu, *Sens. Actuators B* 133, 357, 2008.
- [26] N. K. Singh, S. Shrivastava, S. Rath, S. Annapoorni, *Appl. Surf. Sci.* 257, 1544, 2010.
- [27] L.A. Patil, A.R. Bari, M.D. Shinde, V.V. Deo, D.P. Amalnerkar, *IEEE Sens. J.* 11 (4), 939, 2011.
- [28] Z. Bai, C. Xie, S. Zhang, L. Zhang, Q. Zhang, W. Xu, J. Xu, *Sens. Actuators B* 151 (1), 107, 2010.
- [29] L. J. Bie, X. N. Yan, J. Yin, Y. Q. Duan, Z. H. Yuan, *Sens. Actuators B* 126, 604, 2007.
- [30] L. Yu, X. Fan, L. Qi, L. Ma, W. Yan, *Appl. Surf. Sci.* 257, 3140, 2011.
- [31] A. Diéguez, A. Romano-Rodríguez, J. R. Morante, U. Weimar, M. Schweizer-Berberich, W. Göpel, *Sens. Actuators B* 31, 1, 1996.
- [32] A. A. Firooz, A. R. Mahjoub, A. A. Khodadadi, *Sens. Actuators B* 141, 89, 2009.
- [33] M. V. Vaishampayan, R. G. Deshmukh, I. S. Mulla, *Sens. Actuators B* 131, 665, 2008.
- [34] M. H. Seo, M. Yuasa, T. Kida, J. S. Huh, K. Shimanoe, N. Yamazoe, *Sens. Actuators B* 137, 513, 2009.
- [35] D. Polsongkram, P. Chamninok, S. Pukird, L. Chow, O. Lupan, G. Chai, H. Khallaf, S. Park, A. Schulte, *Physica B* 403, 3713, 2008.
- [36] S. L. Zhang, B. H. Cho, J. B. Yu, J. O. Lim, H. G. Byun, J. S. Huh, *Sens. Lett.* 9, 374, 2011.
- [37] F. Li, Y. Ding, P. X. Gao, X. Q. Xin and Z. L. Wang, *Angew. Chem.* 116, 5350, 2004.
- [38] P. P. Sahay, R. K. Nath, *Sens. Actuators B* 133, 222, 2008.
- [39] N. H. Al-Hardan, M. J. Abdullah, A. A. Aziz, H. Ahmad, L. Y. Low, *Vacuum* 85 (1), 101, 2010.
- [40] N. Hongsith, S. Chooipun, *IEEE Sens. J.* 10 (1), 34, 2010.
- [41] L. K. Bagal, J. Y. Patil, I. S. Mulla, S. S. Suryavanshi, *Ceram. Int.*, doi:10.1016/j.ceramint.2012.02.073, 2012.

**Shao-Lin Zhang** received the master degree in Materials Science and Metallurgy and the Ph.D. degree in Sensor and Display Engineering from the Kyungpook National University, Daegu, Republic of Korea, in 2007 and 2011, respectively. He was Postdoctoral Fellow with the Joint Institute for Regenerative Medicine, Kyungpook National University Hospital, working on the development of gas sensor for medical application. Currently he is a Postdoctoral Fellow at the Department of Materials Science and Engineering in Yonsei University, Seoul, Republic of Korea. His research interests include the design and synthesis of nanomaterials and their application for gas sensor and thermoelectric generator.

**Hyung-Gi Byun** received the BS in Electrical Engineering from Myong-Ji University in 1984, MSc in Electrical Engineering and Electronics, and PhD in Instrumentation and Analytical Science from University of Manchester Institute Science and Technology (UMIST), UK in 1990 and 1995. He joined the Department of Information and Communication Engineering, Kangwon National University, where he is currently a professor with interest in pattern recognition and signal processing based on artificial neural network.

**Jeong-Ok Lim** received her BS degree in Textile Science from Keimyung University, Republic of Korea, in 1981, her MS degree in Biomaterials from Cornell University, USA, in 1988 and her PhD degree in Polymer Science from University of Massachusetts Lowell, USA, in 1993. She is currently a professor at Medical and Biological engineering, Kyungpook National University, Daegu, Republic of Korea. Her major research interests include biomaterials for medical application and conducting polymer membrane assemblies for smart material fabrication.

**Jeong-Soo Huh** received his BS and MS degrees in Metallurgical from the Seoul National University in 1983 and 1985, respectively. He received PhD degree from the Department of Materials Science and Engineering of the Massachusetts Institute and Technology in USA. He is currently a Professor at the Metallurgical Engineering in Kyungpook National University, Daegu,

Republic of Korea. His current research interests are nanomaterials based gas sensor and sensor system for medical application.

**Wooyoung Lee** is a Professor of Department of Materials Science and Engineering, the chairman of Institute of Convergence Technology and the Head of Institute of Nanoscience and Nanotechnology at Yonsei University in Korea. He received a BS degree in metallurgical engineering from the Yonsei University in 1986, a MS degree in metallurgical engineering from the Yonsei University in 1988. He received a Ph.D. degree in Physics from University of Cambridge, England in 2000. He is also the Chairman in University Industrial Technology Force (UNITEF), and a Member of the National Council on Science and Technology. In recent years, his research interests have centered on thermoelectric devices, spintronics and hydrogen sensors based on nanowires. He has received a number of awards in nanodevice-related research areas, including a Service Merit Medal (2008) due to contribution on the development of intellectual properties. He has authored and co-authored over 150 publications, and has edited a few of special books on nano-structured materials and device.